Sintering of titania nanoceramic: Densification and grain growth

Mehdi Mazaheri *, A.M. Zahedi, M. Haghighatzadeh, S.K. Sadrnezhaad

Materials and Energy Research Center, P.O. Box 14155-4777, Tehran, Iran

Abstract

Two-step sintering (TSS) has been applied in the current study to suppress the accelerated grain growth of TiO_2 nanopowder compacts in the final sintering stage. While the grain size ranges between 1 and 2 μm in the full dense structures produced by pressureless conventional sintering (CS), application of two-step sintering has led to a remarkable grain size decline to $\sim$250 nm. With regard to the expensive procedure of spark plasma sintering (SPS), similar density and grain size results determine the straightforward TSS method as a desirable rival for SPS.
© 2008 Elsevier Ltd and Techna Group S.r.l. All rights reserved.

1. Introduction

The outstanding attention that nanostructured materials have recently drawn, stem from their useful mechanical, physical, optical, and magnetic properties [1–6]. These splendid characteristics stimulate several applications in different technological fields such as in electronics, catalysis, magnetic data storage, energy storage, structural components and ceramics [7,8]. The high surface area of nanoparticles, additionally, supplies a substantial sintering driving force by which the sintering temperature can be decently lowered [9–13]. From the mechanical point of view, contrary to the brittleness of micro-grained ceramics, nanometer-grained ones are typically capable of putting up with important elongation before breaking at moderate temperatures ($\sim$0.5 T_m) [7,14].

Nanocrystalline TiO_2 in both forms of powder and compact is an attractive material, applicable to various fields, such as semiconductor photocatalysts for detoxification of environmental pollutants, photovoltaic material for solar energy conversion, structural components for production equipment of semiconductors, pigments, mesoporous membranes, oxygen sensors, and as a major constituent of many dielectric materials [15]. TiO_2 ceramics are also of a great efficiency in the low

temperature creep [16]. Due to the larger specific surface area of the ultrafine-grained titanium dioxide, they demonstrate a superb photocatalytic performance [17,18]. Application of an efficient sintering procedure, therefore, plays a crucial role in producing near full dense TiO_2 structures with a fine grain size. Several sintering methods including conventional sintering (CS), spark plasma sintering (SPS), millimeter-wave radiation, hot pressing (HP) and sinter forging have already been employed to derive full dense TiO_2 bodies [19–25]. Pressureless conventional sintering (CS) is the most common low cost approach to sinter the ceramics among all of the mentioned methods. This method is generally incapable of preparing full dense ultrafine-grained ceramics. The reason lies in this fact that, grain growth and densification are both driven by diffusive mechanisms which result to the simultaneous activation of densification and grain growth in the later stage of sintering [19]. After the density of 90% of theoretical density (TD), grains can grow when the continuous network of pores breaks down on grain boundaries and a drastic grain size evolution is expected in conventionally sintered specimens [9,24]. Siegel et al. [26] and Hahn et al. [27] have pressureless sintered nanophase TiO_2 and obtained samples with a submicrometer average grain size. Apropos of the abovementioned instance, one can realize the importance of hiring a promising consolidation technique to avoid exaggerated grain growth at the final stage of sintering. According to the theoretical literature, sintering principles depend on parameters like temperature, pressure, particle size, and doping. Pressure-assisted methods such as HP and SPS are reported to be advantageous for curbing the grain size evolution [21,22,24,27].

* Corresponding author at: Materials and Energy Research Center, P.O. Box 14155-4777, Tehran, Iran. Tel.: +98 912 1691309, fax: +98 261 4412303.

E-mail addresses: mazaheri@merc.ac.ir, mmazaheri@gmail.com (M. Mazaheri).

Angerer et al. [22], instantly, gained a near full dense TiO_2 structure, using CS method, by primary particle size of 40 nm, however, the final grain size was >1 µm. In contrast, they [22] have reported such a full dense structure with finer grains (~120 nm) using SPS. Lee et al. [21] also obtained a full dense structure with the average grain size of ~200 nm, using the well-known Degussa Co., TiO_2 nanopowder. HP also appears as an appropriate technique to densify ceramics with a controlled grain growth. Hahn et al. [27], for example, have reported an enhancement of sintering with a slight grain size increase after applying pressure. Microstructural investigations have revealed two different phases in TiO_2 structures through the sintering procedure, i.e. anatase as the low temperature stabilized phase and rutile which is the result of anatase transformation at ~600 °C [19]. Weibel et al. [7,24] have applied HP at rather low temperatures to obtain near full dense anatase-stabilized compacts. They have explored the optimization of applied pressure and temperature to keep the small grain size in the initial anatase phase by sintering at low temperatures [24]. Plenty of researches [19,20,28,29] have furthermore, exposed transformation (anatase to rutile) assisted sintering as a gifted route to derive high dense titania nanostructures. Liao et al. [30], as well as Mazaheri et al. [31], using phase-transformation-assisted sintering method, came to this conclusion that grain growth is possibly restricted by the low sintering temperature and TiO_2 phase transformation depending on the combination of high pressure and low temperature. Li et al. [20], besides, employed CS assisted by phase-transformation to obtain bulk TiO_2 ceramics with the final density of 95% and average grain size of <60 nm using sol–gel synthesized anatase nanopowders (7–38 nm). Kumar et al. [19], have reported the achievement of >99% TD for titania nanostructures with an average grain size of <60 nm, by sintering a titanium oxide sol–gel near the anatase to rutile transformation temperature.

In addition to the aforementioned well-known sintering methods in TiO_2 system, another way to control grain growth at the sintering later stage is the two-step sintering (TSS) method, made public first by Chen and Wang [32] as a novel pressureless technique. It is a promising approach to obtain full dense nanostructured ceramics. This method modifies sintering regimes by high temperature (T_1) firing followed by rapid cooling and low temperature (T_2) soaking of the samples [9,32–34]. In addition to Y_2O_3, Ni–Cu–Zn ferrite, $BaTiO_3$ by Wang et al. [33,34], Mazaheri et al. [9,13,35] have recently applied this method on nanocrystalline ZnO, 8YSZ and 3Y-TZP successfully.

In the present work, it has been attempted to verify the applicability of TSS process for TiO_2 nanostructures. The densification and grain growth results of samples sintered by CS and TSS were compared with the available results of SPS method found in the literature.

2. Experimental procedure

2.1. Raw material

TiO_2 nanopowder (P25, Degussa Co., Frankfurt, Germany) with the particle size between 11 and 27 nm (Fig. 1(a),

TEM, CM200 FEG, Philips, Netherlands) and the specific surface area (BET, Micromeretics Gemini 2375, USA) of 55.3 $m^2 g^{-1}$ was selected as the starting material. Phase content of as-received powder was calculated from XRD pattern (Fig. 1(b)) with Cu Kα radiation (Philips X'Pert, Netherlands) to distinguish anatase and rutile phases via their peak intensities (described in detail elsewhere [36]). The value of anatase and rutile phases was found to be 77% and 23%, respectively, in the composition of starting powder. The crystallite size of the anatase and rutile phases was determined to be 21.7 and 14.5 nm, respectively, based on Scherrer equation [37].

2.2. Compaction

The powder was uniaxially pressed at 100 MPa into the pellets of 5-mm diameter and ~3-mm thickness. After ejection of the compacts from the die, the green density of the pellets was determined to be ~0.53 of TD using volumetric method. This method consists of measuring weight and dimensions of the compacts by using an accurate balance (10^{-5} g) and a micrometer (10^{-5} m).

The compressibility of the as-received powder was, also, evaluated by pressing the as-received powder at the range of applied pressures between 10 and 100 MPa. The green density of compacts was, then, evaluated using the above method.
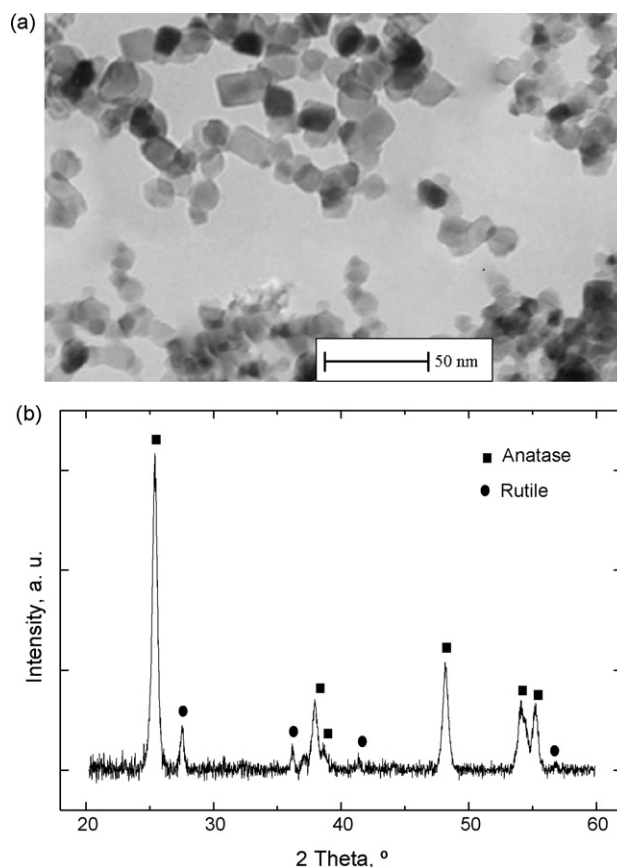

Fig. 1. (a) Transmission electron microscopy (TEM) micrograph and (b) X-ray diffraction (XRD) pattern of as-received TiO_2 nanopowder.

2.3. Sintering

Sintering of green bodies was carried out by CS and TSS methods. CS specimens were sintered between 500 and 1000 °C for 1 h in air with a heating ramp of 5 °C min^{-1}. For the first step of TSS, samples were heated under the same conditions as CS. After being held at a higher temperature (T_1) for 1 h, samples were cooled from T_1 (800 °C) to T_2 (700 °C) with a cooling rate of 50 °C min^{-1}. The samples were, then, soaked at T_2 up to 25 h. The density of the sintered samples was measured by the water displacement (Archimedes) method. Regards to the bi-phasal composition of titania pellets, the specimens are made up of rutile and anatase phases with different theoretical densities. The TD of such composite, therefore, was measured based on the rule of mixture, using phase fraction of rutile and anatase and their TD (4.26 and 3.84 g cm^{-3}, respectively).

2.4. Microstructural characterization

For microstructural characterization, sintered pellets were fractured and then studied using SEM (Philips XL30, Netherlands). An image analyzer calculated the mean grain size of the samples. To determine the amount of density and grain size of the specimens, three samples were at least used and the average value was reported in results. XRD analysis was performed using Cu Kα on sintered samples to determine microstructural phases. A continuous step scanning XRD analysis was conducted in the 2θ range of 20–30° at step size of 0.01° using PW3710-based Philips diffractometer to investigate the existence of any major peak associated with rutile (2θ = 27.5°) or anatase (2θ = 25.4°).

3. Results and discussion

3.1. Compaction

One of the most crucial features for producing near full dense ceramics is the powder compressibility, by which the compact green density and therefore the fired density are directly contributed. Applying a ceramic powder with a good potential of compression can lead to a lower sintering temperature and therefore accessing an ultrafine structure. Microstructure and size distribution of the particles, in addition to the presence of agglomerates, play a significant role in a proper densification process [35]. According to Khasanov et al. [38], an appropriate compaction route must eliminate the requirement of employing binders or plasticizers for consolidation affairs as the notorious source of impurities. The powder compressibility, regards to Khasanov instructions, is evidently influenced by key elements like P_{cr} and b in the following equation:

$$\rho = b \ln \left(\frac{P_{pr}}{P_{cr}} \right) + 1 \tag{1}$$

where ρ is the relative density of green compact, P_{pr} is the compaction pressure and P_{cr} as well as b are introduced as "the

critical compaction pressure at which the void free condition of a green compact is reached" and "the constant describing densification intensity of the compact powder", respectively. Higher b accompanying with a low P_{cr} can lead to an optimum compaction circumstances [38]. Fig. 2 shows the green density dependency of titania compacts on applied pressure in log scale. As the figure depicts, the more pressure exerted on the powder, the more green density is provided for compacts. The very prominent feature is the existence of an intersection point (P_y) on the plot, after which the slope changes and density increases faster in return of adding to the applied pressure. Regarding to the following equation:

$$\frac{d \rho}{d \ln P_{cr}} = b \tag{2}$$

The parameter b is the slope of diagram and, decently, reflects the compaction behavior of a powder in a wide range of applied pressure. According to the above explanations and the sharper slope of the diagram after the intersection point ($P_y \approx 37$ MPa), one can deduce a better compressibility for the powder at the right section of the compaction curve. Our calculations also, verify a higher b and a lower P_{cr} for the applied pressures higher than P_y in comparison with the left section of the graph. The results of calculations are totally represented in Table 1. While the value of b increases from 0.036 to 0.177 soon after the applied pressure excesses ∼37 MPa (P_y), the critical pressure (P_{cr}) reduces to 1.41×10^3 after the abrupt change of the slope. This sudden variation, however, deserves more exploration in the literature. There are numerous other investigations targeting at reaction of different powders against compaction. Groot Zevert et al. [39] charge the agglomeration of powder responsible for the mentioned observation. After compaction at a pressure around P_y, the agglomerates are gradually fragmented, and their rearrangement becomes feasible at lower pressures [35]. The accuracy of this theory is well confirmed by Srdic et al. [40]. They compacted two differently synthesized powders and plotted their green density–pressure trajectories. In the case of nonagglomerated powder, compaction behavior is
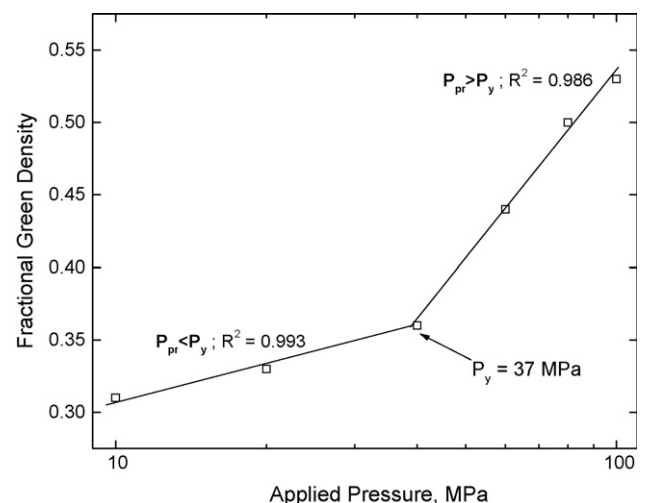
Fig. 2. Densification behavior of TiO$_2$ nanopowder as a function of the applied pressure: P_y refers to the strength of the agglomerates.

Table 1
Compressibility parameters of TiO_2 nanopowder

Applied pressure range, P_{pr}	Compressibility intensity, b	Critical pressure, P_{cr}	Correlation coefficient, R^2
$P_{pr} < P_y$	0.036	2.23×10^9	0.993
$P_{pr} > P_y$	0.177	1.41×10^3	0.986

ironically described by a simple logarithmic correlation within the applied pressure range. The agglomerated one, on the contrary, exhibits two logarithmic dependencies with a point of intersection [40].

3.2. Conventional sintering

The changes of fractional density and grain size of conventionally sintered samples with temperature are shown in Fig. 3. As can be seen, while the sintering rate increases dramatically between 650 and 800 °C and the density enhances to 0.91 of TD through the second stage of sintering, the grain size does not show a remarkable change. In contrast, after the beginning of the sintering final stage, more temperature excess from 800 to 1000 °C retards (slows down) densification and results to an abrupt grain size increase. As the diffusion arouses both densification and grain growth, and regards to the temperature dependency of diffusive mechanisms, the temperature increase between 800 and 1000 °C will definitely impose a simultaneous advance in density and grain size on the sintering later stage [41]. One may question that in spite of the identical temperature increase from 650 to 800 °C how we can describe the continuation of densification without any noteworthy grain growth. The reason lies in the magnificent pore pinning phenomenon, according to which the grain boundaries are dragged by the connected network of pores thorough the second stage of sintering. With the beginning of the final stage, however, the abovementioned connected network disintegrates and open pores collapse to the closed ones. Such a situation leads to the leisure movement of grain boundaries and therefore a predicable drastic grain growth [9,25,32]. Gas pressure within pores, besides, hinders a proper densification in the final stage of sintering [42]. Therefore, the

grain growth eventually dominates above 800 °C and results to a disapproved microstructural coarsening. As the authors have indicated elsewhere [9], microstructural coarsening; including grain and pore growth, is commonly described by an interaction between coarsening and densification. The coarsening ultimately dominates and leads to an incredible decline in sintering rate (above 850 °C) [43].

3.3. Two-step sintering

Fig. 4 illustrates variation of density and grain size versus the holding time in TSS second step. The temperature and the holding time of the first (T_1) and the second step (T_2) of TSS are 800 °C for 1 h and 700 °C for 25 h, respectively. As shown in this figure, the density becomes ∼91% TD and the grain size reaches 188 nm after the first step of TSS. Holding the specimens at 700 °C up to 25 h results to a remarkable fractional density increase from 0.91 to ∼0.98 while the grain size does not show any notable evolution. The period during which such steep density increase coincides an ignorable grain size variation is called "incubation time" by Wang et al. [33,34] and takes place in the TSS second step. As indicated by several investigators [9,32–35], the above incident relates to the act of boundary dragging by junctions in the second step of TSS. Mazaheri et al. [9,35], additionally, have shown elsewhere that the junction density, at the end of first step, directly influences the incubation time. It is, therefore, concluded that a lower junction density than a critical value does not lead to an enough incubation time. Before reaching a full dense structure, hence, an abrupt grain growth triggers [9]. As shown in Fig. 4, holding time of 25 h is long enough to result in a full dense structure without a significant grain growth. The reason lies in the small value of grain size (188 nm) resulting to a high density
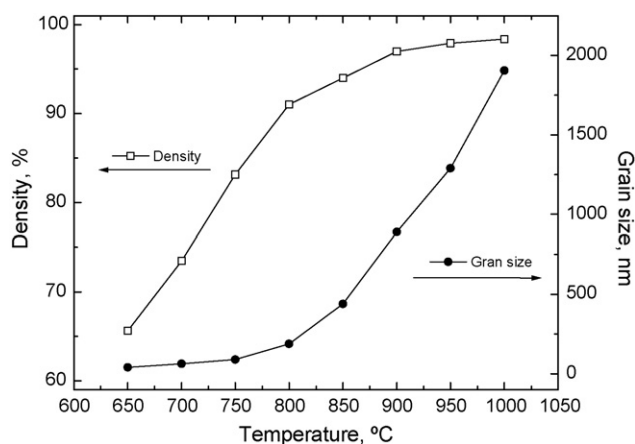

Fig. 3. Density and grain size of conventionally sintered TiO_2 nanostructures as a function of sintering temperature.
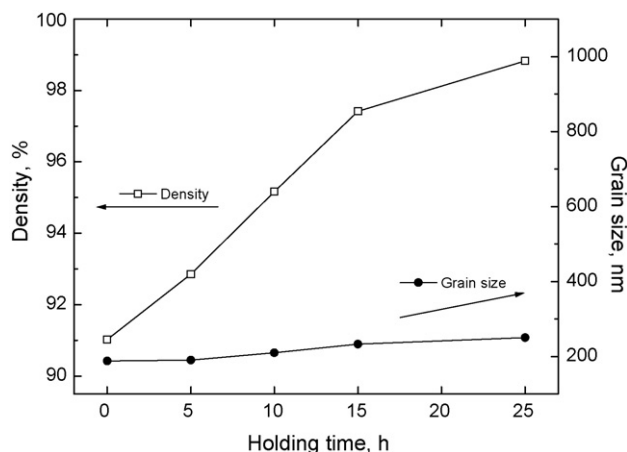

Fig. 4. Density and grain size of the specimens sintered under TSS conditions versus holding time at 700 °C.

of junctions at the end of first step. Canadian scientists [44] have proved that for large grain sizes, triple junction volume fraction is ignorable in comparison with the total interface volume fraction. One can infer that the intercrystalline volume fraction is almost made up of grain boundary atoms in large grain sizes. Due to the stronger grain size dependence of the smaller grains, however, the volume fraction of the smaller grains tends to increase much faster with the grain size reduction than the grain boundary volume fraction. For the very small grains, therefore, triple junction contribution ultimately dominates over the grain boundary one [44].

Fig. 5 depicts the fracture surfaces of full dense specimens sintered by CS and TSS regimes. The very prominent feature in SEM figures is the intergranular fracture which is the common element of both conventionally and two-step sintered samples. The grain size difference, however, is the most distinctive criterion between two aforementioned structures.

Fig. 6 displays the grain size/relative density trajectory of tested sintering regimes. In order to have a better comparison, results of samples sintered by SPS and CS, reported by Lee et al. [21], are also represented in the aforementioned picture. In terms of CS graph, in densities below 90% TD, boundary dragging by the open pores in second sintering stage deters the grain growth. In contrast, collapse of the open pores in the last stage leads to an abrupt grain growth above 90% TD [25,41,42]. Regards to the similar initial powder and equal green density, our results are in a good agreement with those of reported by
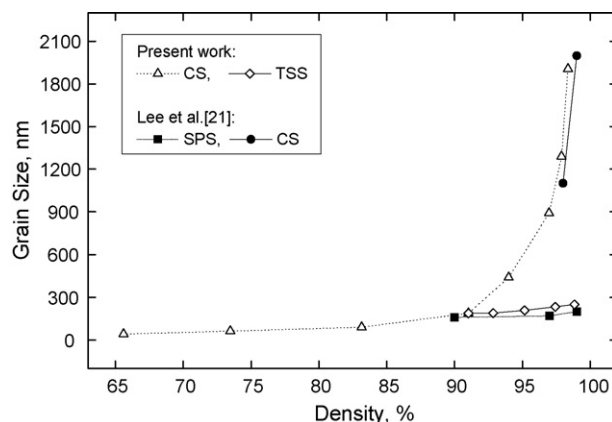
Fig. 6. Grain size-density diagrams of the specimens sintered by CS, SPS and TSS methods.

Lee et al. [21]. The SPS results indicate notable grain growth suppression in addition to achieving a density >98% TD with the grain size of 200–300 nm. This fact accompanied by the simultaneous application of three mechanisms (a) uniaxial pressing, (b) pulsed voltage and (c) resistance heating of graphite dies, have turned SPS into a favorite method to produce nanostructured ceramics [21,22]. On the other hand, this route despite being expensive and unavailable does not result in better consequences than TSS. The TSS regime in the present work causes near full dense structures with the grain size of ~250 nm. Furthermore, TSS represents its dazzling outgoings with quite available facilities like a pressureless sintering furnace. The authors have, elsewhere [9], explained the mechanism of grain growth suppression via TSS, mostly based on Chen and Wang [32] alleges. They believe that the low temperature of TSS second step impedes the triple junction mobility and their stagnancy can solidly prohibit the grain boundary migration. Czubayko et al. [45], have also confirmed the accuracy of the abovementioned theory. They have reported, in their investigation, that the activation enthalpy of triple junctions is definitely constant over the entire temperature interval. The value of triple junction mobility, also, increases abruptly via rising temperature. They have declared that the activation enthalpy of triple junctions' migration is higher than one for grain boundary mobility. The temperature excess can, hence, provide the chance of being more mobile for triple junctions compared to the grain boundaries due to a higher activation enthalpy of migration. The boundaries, in this case, can move freely without any obstacle and result to a widespread and dangerous grain growth. The grain boundary mobility, as a process with the lower activation enthalpy, controls the motion of the boundary system at high temperatures. At relatively low temperatures, however, the boundaries' motion is governed by the reduced mobility of the triple junctions. Contrary to the grain boundary motion, triple junction migration is not only influenced by the intrinsic mobility but also the grain size. The grain size increase can provide a higher value of mobility for triple junctions [45]. The low temperature of TSS second step, nevertheless, prepares small grains and, hence, less value of mobility for triple
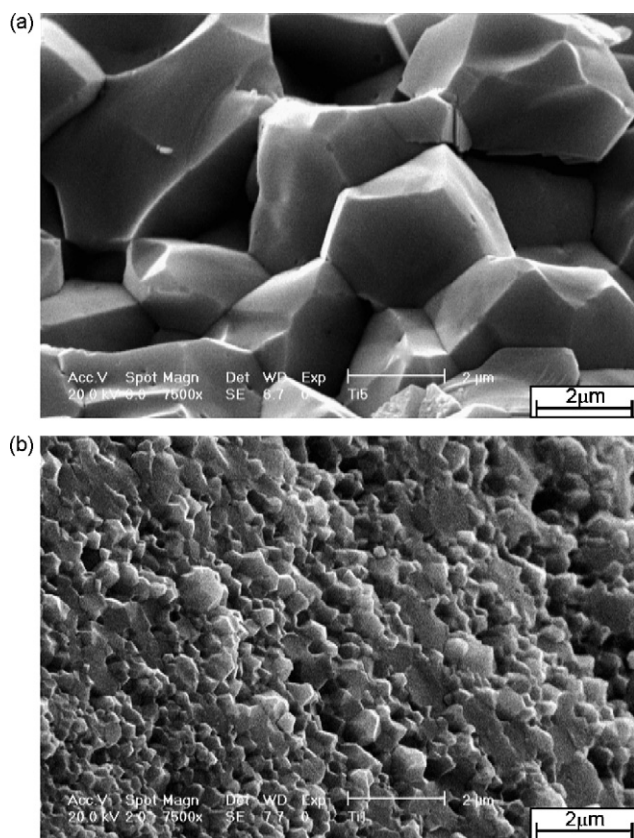
Fig. 5. Scanning electron microscopy micrographs relating fracture surfaces of specimens obtained by (a) CS at 1000 °C for 1 h and (b) TSS at 800 °C for 1 h then 700 °C for 25 h.
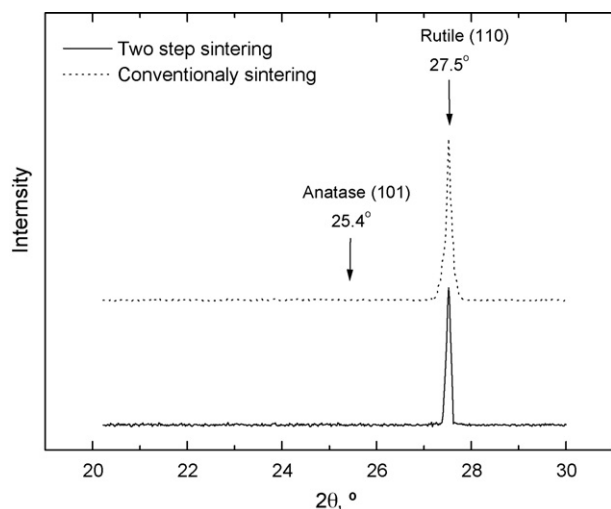
Fig. 7. X-ray diffraction (XRD) pattern of two-step and conventionally sintered microstructures in the 2θ range between $20°$ and $30°$: the highest peak in each pattern reflects the presence of rutile as the major microstructural phase.

junctions. Because the absolute value of triple junction mobility and its migration rate are evidently lower for fine-grained structures, dragging of grain boundaries by the hardly mobile junctions as well as superb grain growth suppression can be decently performed via sintering at TSS second step.

There are plentiful investigations available, openly reporting a kind of transformation phenomenon likely to happen from the anatase to rutile phase thorough the sintering of TiO_2 systems [19,20,28]. The CS sintering temperature in the current study is much higher than the real transformation temperature (600 °C). Rutile, thus, must be the only phase present in full dense samples obtained by this route. Apropos of SPS, the pressure used during the mechanism results to a complete rutile microstructure [22]. Because applying a high pressure sintering procedure is another way to stimulate the anatase to rutile conversion [28]. Fig. 7 represents the X-ray diffraction (XRD) pattern of two-step and conventionally sintered microstructures in the 2θ range between $20°$ and $30°$. As the peak with the highest intensity relates to the rutile phase, TSS microstructure is also exposed to be consisting of rutile as the major phase. In spite of the low temperature of the second step in TSS, prolonged annealing time in this temperature (25 h) by which the kinetic effect is activated, allows a complete anatase to rutile transformation.

4. Conclusion

1. The application of TSS on the pressed TiO_2 nanostructures prohibits the grain growth in the final stage of sintering. While CS produces full dense structures with the grain size of 1–2 μm, TSS reduces the mentioned value to ∼250 nm.
2. A comparison of TSS density/grain size results is carried out with those for SPS. The economical verification of using SPS comes in to the question when the simple rout of TSS leads to the full dense structures with decent grain growth suppression.
3. Due to having a higher enthalpy of activation, triple junction mobility plays the role of a controlling mechanism at rather

low temperatures. Grain boundary mobility, therefore, is severely inhibited by the stagnancy of triple junctions and the process leads to magnificent ultrafine structures.

References

[1] R. Vaben, D. Stover, Processing and properties of nanophase ceramics, Journal of Materials Processing Technology 92 (1999) 77–84.
[2] M. Salavati-Niasari, F. Davar, M. Mazaheri, M. Shaterian, Preparation of cobalt nanoparticles from [bis(salicylidene)cobalt(II)]–oleylamine complex by thermal decomposition, Journal of Magnetism and Magnetic Materials 320 (2007) 575–578.
[3] J. Karch, R. Brringer, H. Gleiter, Ceramics ductile at low temperatures, Nature 330 (1987) 556–558.
[4] M.J. Mayo, D.C. Hague, D.J. Chen, Processing Nanocrystalline Ceramics for Application in Superplasticity, Material Science and Engineering A 166 (1993) 145–159.
[5] M.J. Mayo, Synthesis and applications of nanocrystalline ceramics, Materials and Design 14 (1993) 323–329.
[6] Y. Sakka, T.S. Suzuki, K. Morita, K. Nakano, K. Hiraga, Colloidal processing and superplastic properties of zirconia and alumina-based nanocomposites, Scripta Materialia 44 (2001) 2075–2078.
[7] A. Weibel, R. Bouchet, P. Bouvier, P. Knauth, Hot compaction of nanocrystalline TiO_2 (anatase) ceramics mechanisms of densification: grain size and doping effects, Acta Materialia 54 (2006) 3575–3583.
[8] S. Yang, L. Gao, Preparation of titanium dioxide nanocrystallite with high photocatalytic activities, Journal of the American Ceramic Society 88 (2005) 968–970.
[9] M. Mazaheri, A.M. Zahedi, S.K. Sadrnezhaad, Two-step sintering of nanocrystalline ZnO compacts: effect of temperature on densification and grain growth, Journal of the American Ceramics Society 91 (2008) 56–63.
[10] J.R. Groza, Nanosintering, Nanostructured Materials 12 (1999) 987–992.
[11] K. Maca, M. Trunec, P. Dobask, Bulk zirconia nanoceramics prepared by cold isostatic pressing and pressureless sintering, Reviews on Advanced Materials Science 10 (2005) 84–88.
[12] D. Jiang, M.J. Mayo, Rapid rate sintering of nanocrystalline ZrO_2–3 mol.% Y_2O_3, Journal of the American Ceramic Society 79 (1996) 906–912.
[13] M. Mazaheri, A. Simchi, F.G. Fard, Master Densification and grain growth of nanocrystalline 3Y-TZP during two-step sintering , Journal of the European Ceramic Society, in press.
[14] M.J. Mayo, D.J. Chen, D.C. Hague, in: A.S. Edelstein, R.C. Cammarata (Eds.), Nanomaterials: Synthesis, Properties and Applications, Institute of Physics Publishing, Bristol, UK, 1996, p. 191.
[15] C.-K. Shin, Y.-K. Paek, Effect of CuO on the sintering behavior and dielectric characteristics of titanium dioxide, International Journal of Applied Ceramic Technology 3 (2006) 463–469.
[16] H. Hahn, R.S. Averback, Low-temperature creep of nanocrystalline titanium (IV) oxide, Journal of the American Ceramic Society 74 (1991) 2918–2921.
[17] C.J. Barbe, F. Arendse, P. Comte, M. Jirousek, F. Lenzmann, V. Shoklover, M. Gratzel, Nanocrystalline titanium oxide electrodes for photovoltaic applications, Journal of the American Ceramic Society 80 (1997) 3157–3171.
[18] M. Gratzel, Perspectives for dye-sensitized nanocrystalline solar cells, Progress in Photovoltaics: Research and Applications 8 (2000) 171–185.

[19] K.P. Kumar, K. Keizer, A.J. Burggraaf, T. Okubo, H. Nagamoto, S. Morooka, Densification of nanostructured titania assisted by a phase transformation, Nature 358 (1992) 48–51.

[20] J. Li, Y. Yea, L. Shen, J. Chen, H. Zhou, Densification and grain growth during pressureless sintering of TiO_2 nanoceramics, Materials Science and Engineering A 390 (2005) 265–270.

[21] Y.I. Lee, J.-H. Lee, S.-H. Hong, D.-Y. Kim, Preparation of nanostructured TiO_2 ceramics by spark plasma sintering, Materials Research Bulletin 38 (2003) 925–930.

[22] P. Angerer, L.G. Yu, K.A. Khor, G. Krumpel, Spark-plasma-sintering (SPS) of nanostructured and submicron titanium oxide powders, Material Science and Engineering A 381 (2004) 16–19.

[23] N. Masahashi, Fabrication of bulk anatase TiO_2 by the spark plasma sintering method, Materials Science and Engineering A 452/453 (2007) 721–726.

[24] A. Weibel, R. Bouchet, R. Denoyel, P. Knauth, Hot pressing of nanocrystalline TiO_2 (anatase) ceramics with controlled microstructure, Journal of European Ceramic Society 27 (2007) 2641–2646.

[25] S.-J.L. Kang, Sintering Densification, Grain Growth and Microstructure, Elsevier, Oxford, 2005.

[26] R.W. Siegel, S. Ramasamy, H. Hahn, L. Zongquan, L. Ting, Synthesis, characterization, and properties of nanophase TiO_2, Journal of Materials Research 3 (1988) 1367–1372.

[27] H. Hahn, J. Loga, R.S. Averback, Sintering characteristics of nanocrystalline TiO_2, Journal of Materials Research 5 (1990) 609–614.

[28] S.-C. Liao, Y.-J. Chen, W.E. Mayo, B.H. Kear, Transformation-assisted consolidation of bulk nanocrystalline TiO_2, Nanotructured Materials 11 (1999) 553–557.

[29] R.-G. Duan, G.-D. Zhan, J.D. Kuntz, B.H. Kear, A.K. Mukherjee, Processing and microstructure of high-pressure consolidated ceramic nanocomposites, Scripta Materialia 51 (2004) 1135–1139.

[30] S.C. Liao, W.E. Mayo, K.D. Pae, Theory of high pressure/low temperature sintering of bulk nanocrystalline TiO_2, Acta Materialia 45 (1997) 4027–4040.

[31] M. Mazaheri, Z. Razavi Hesabi, S.K. Sadrnezhaad, Two-step sintering of titania nanoceramics assisted by anatase-to-rutile phase transformation, Scripta Materialia 59 (2008) 139–142.

[32] I.-W. Chen, X.-H. Wang, Sintering dense nanocrystalline oxide with-out final stage grain growth, Nature 404 (2000) 168–171.

[33] X.H. Wang, P.L. Chen, I.W. Chen, Two-step sintering of ceramics with constant grain-size, I. Y_2O_3, Journal of the American Ceramic Society 89 (2006) 431–437.

[34] X.-H. Wang, X.Y. Deng, H.-L. Bai, H. Zhou, W.-G. Qu, L.T. Li, I.-W. Chen, Two-step sintering of ceramics with constant grain-size II BaTiO3 and Ni–Cu–Zn ferrite, Journal of the American Ceramic Socity 89 (2006) 438–443.

[35] M. Mazaheri, M. Valefi, Z. Razavi Hesabi, S.K. Sadrnezhaad, Two-step sintering of nanocrystalline $8Y_2O_3$ stabilized ZrO_2 synthesized by glycine nitrate, Ceramics International, in press.

[36] J.F. Porter, Y.–G. Li, C.K. Chan, The effect of calcination on the microstructural characteristics and photoreactivity of Degussa P-25 TiO_2, Journal of Materials Science 34 (1999) 1523–1531.

[37] B.D. Cullity, Diffraction I: Directions of Diffracted Beams, Elements of X-ray Diffraction, 2nd ed., Addison-Wesley Publishing Company, Inc., Massachusetts, 1978, pp. 100–103.

[38] O.L. Khasanov, E.S. Dvilis, V.M. Sokolov, Compressibility of the structural and functional ceramic nanopowders, Journal of the European Ceramic Society 27 (2007) 749–752.

[39] W.F.M. Groot Zevert, A.J.A. Winnubst, G.S.A.M. Theunissen, A.J. Burggraaf, Powder preparation and compaction behavior of fine-grained Y-TZP, Journal of Materials Science 25 (1990) 3449–3455.

[40] V.V. Srdic, M. Winterer, H. Hahn, Sintering behavior of nanocrystalline zirconia prepared by chemical vapor synthesis, Journal of the American Ceramic Society 83 (2000) 729–736.

[41] R.M. German, Powder Metallurgy Science, Metal Powder Industries Federation, Princeton, NJ, 1984.

[42] M.N. Rahaman, Ceramic Processing and Sintering, 2nd ed., Marcel-Dekker Inc., New York, 2003.

[43] A.P. Hynes, R.H. Doremus, R.W. Siegel, Sintering and characterization of nanophase zinc oxide, Journal of the American Ceramic Society 85 (2002) 1979–1987.

[44] Y. Zhou, U. Erb, K.T. Aust, G. Palumbo, The effects of triple junctions and grain boundaries on hardness and Young modulus in nanostructured Ni–P, Scripta Materialia 48 (2003) 825–830.

[45] U. Czubayko, V.G. Sursaeva, G. Gottstein, L.S. Shvindlerman, Influence of Triple junctions on grain boundary motion, Acta Materialia 46 (1998) 5863–5871.